Dalton Transactions

Accepted Manuscript

ROYAL SOCIETY OF CHEMISTRY

www.rsc.org/dalton

Mechanisms of Ni *N*-Heterocyclic Carbene Catalysts for C-O Bond Hydrogenolysis of Diphenyl Ether: A Density Functional Study

Boodsarin Sawatlon,[‡a] *Taveechai Wititsuwannakul,*[‡a] *Yuthana Tantirungrotechai,*[c] *and Panida Surawatanawong,**[a,b]

[a]Department of Chemistry and Center of Excellence for Innovation in Chemistry, Faculty of Science, Mahidol University, 272 Rama VI Road, Ratchathewi, Bangkok 10400, Thailand.

[b]Center for Alternative Energy, Mahidol University, 999 Phuttamonthon 4 Road, Salaya, Nakhon Pathom 73170, Thailand.

[c]Department of Chemistry, Faculty of Science, Thammasat University, Thailand

[‡]These authors contributed equally to this work.

*E-mail: panida.sur@mahidol.ac.th

Table of Contents Graphic

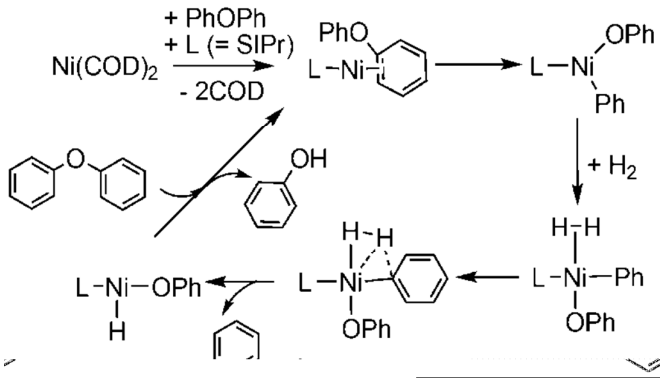

Ni(SIPr)(η^2-PhOPh) is the key active species for C-O bond hydrogenolysis of diphenyl ether.

ABSTRACT

Catalysts for aromatic C-O bond activation can potentially be used for the lignin degradation process. We investigated the mechanisms of C-O bond hydrogenolysis of diphenyl ether (PhOPh) by the nickel *N*-heterocyclic carbene (Ni-SIPr) complex to produce benzene and phenol as products. Our calculations revealed that diphenyl ether is not only a substrate, but also serves as a ligand to stabilize the Ni-SIPr complex. The Ni(SIPr)(η^6-PhOPh) complex is initially formed before rearranges to Ni(SIPr)(η^2-PhOPh), the active species for C-O bond activation. The catalytic reaction has three steps: (i) oxidative addition of Ni(SIPr)(η^2-PhOPh) to form $[Ni(SIPr)(OPh)(Ph)]^0$, (ii) σ-complex-assisted metathesis, in which H_2 binds to the nickel to form $[Ni(SIPr)(OPh)(Ph)(H_2)]^0$, then benzene (or phenol) is eliminated, and (iii) reductive elimination of phenol (or benzene) and the binding of PhOPh to regenerate Ni(SIPr)(η^2-PhOPh). As the rate determining step is at the oxidative addition step (+24 kcal/mol), we also calculated the free energy barriers for the oxidative addition of diaryl ether containing a trifluoromethyl electron withdrawing group ($PhOC_6H_4CF_3$) and found that C-O bond activation at the carbon adjacent to the aryl ring that contains the electron withdrawing substituent is preferred. This is in agreement with the experimental results, in that the major products are phenol and trifluoromethylbenzene. Moreover, the hydrogenation of benzene *via* Ni(SIPr)(η^2-C_6H_6) requires a high energy barrier (+39 kcal/mol); correspondingly, the hydrogenation products, e.g., cyclohexane and cyclohexadiene, were not observed in the experiment. Understanding the reaction mechanisms of the nickel catalysts for C-O bond hydrogenolysis of diphenyl ether will guide the development of catalytic systems for aromatic C-O bond activation to achieve the highest possible selectivity and efficiency.

INTRODUCTION

Catalysts for aromatic C-O bond activation are significant for the conversion of lignin biomass to arene feedstocks.[1, 2] Wenkert *et al*. first reported the cross-coupling reaction of aryl methyl ether and phenyl Grignard reagents using a $NiCl_2(PPh_3)_2$ catalyst.[3] Apart from Grignard reagents,[4, 5] other carbon nucleophiles, e.g., organozinc[6] and arylboronic reagents,[7-9] have been used for C-O bond activation. Despite being less reactive, hydrogen attracted much attention for use as a substrate in place of the carbon nucleophile.

Hydrogenolysis of aromatic C-O bonds can be done by a heterogeneous Ni catalyst.[10] However, its high reactivity results in further hydrogenation of the product, which leads to product mixtures of arenes and alcohols as well as cycloalkanes and cycloalkanols.[1, 10] Recently, Sergeev and Hartwig[2] reported that the nickel *N*-heterocyclic carbene complex (Ni-SIPr) (Scheme 1) can catalyze hydrogenolysis of diaryl ethers[2] to produce arenes and alcohols as products. The reaction of the diaryl ether containing an electron withdrawing trifluoromethyl group can proceed at a lower temperature than the unsubstituted diphenyl ether and diaryl ethers with an electron donating group. In a competition experiment in which both diphenyl ether and 4-*tert*-butylphenyl methyl ether are present, C-O bond hydrogenolysis for the diphenyl ether was preferred (Scheme 1). As lignin contains aromatic C-O bonds, which are generally difficult to activate, this selective catalytic system could have promising applications in lignin degradation.

Density functional theory (DFT) can complement experimental studies to give insights into the reaction mechanisms of C-O bond activation by Ni complexes.[11, 12] Shi and coworkers[7] reported that $Ni(PCy_3)_2Cl_2$ can selectively activate the aryl C-O bond (Ar-OAc) in the reaction of a series of aryl esters with arylboronic reagents to obtain biaryl products, although the acyl C-O bond (ArO-Ac) is weaker and normally perceived to be activated first. Liu and coworkers[13] performed density functional study on the mechanisms and revealed that although the oxidative addition of ArO-Ac to the Ni^0 complex is more facile than the oxidative addition of Ar-OAc, the subsequent transmetalation step for the former needs to overcome a higher energy barrier.

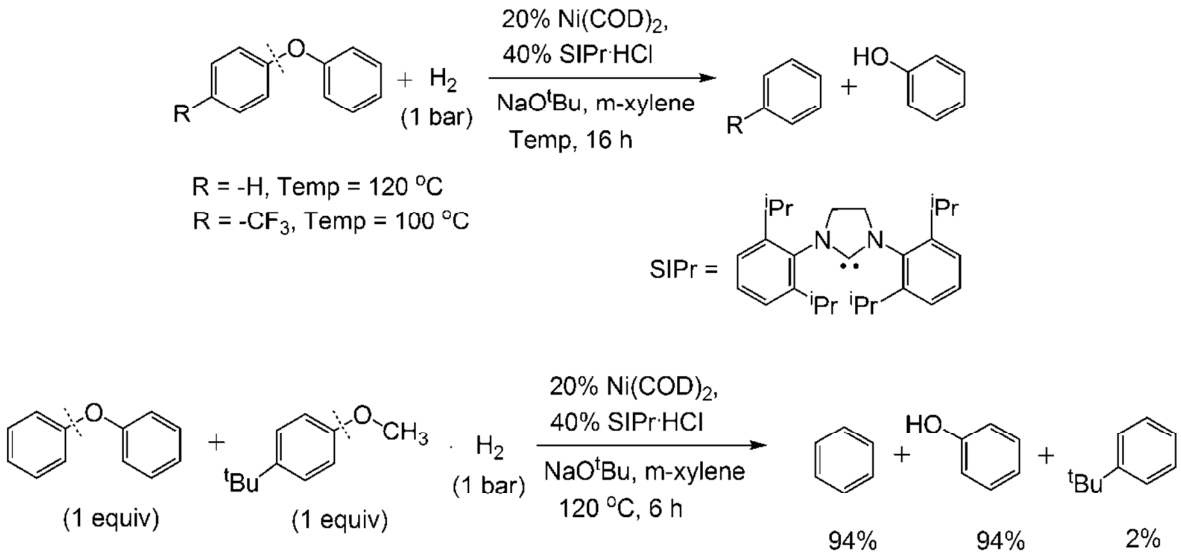

Scheme 1. Ni-SIPr reactions for C-O bond hydrogenolysis of diaryl ethers.

In this study, we used density functional theory to study the mechanism of the Ni-SIPr catalyst for the hydrogenolysis of the C-O bond of diphenyl ether (PhOPh). In the catalytic reaction between PhOPh and H_2 using $Ni(COD)_2$ and SIPr·HCl in the presence of *tert*-butoxide base, Ni(SIPr)(η^6-PhOPh) can be formed and rearranged to Ni(SIPr)(η^2-PhOPh), the active species. The reaction mechanisms and the key species were investigated (Scheme 2). The catalytic cycle has three steps: (i) oxidative addition of Ni(SIPr)(η^2-PhOPh) to form $[Ni(SIPr)(OPh)(Ph)]^0$, (ii) σ-complex-assisted metathesis (σ-CAM), in which H_2 binds to the nickel and benzene (or phenol) is eliminated, and (iii) reductive elimination of phenol (or benzene) and rebinding of PhOPh to recover Ni(SIPr)(η^2-PhOPh). Understanding the reaction mechanisms of the nickel catalysts for C-O bond hydrogenolysis of diphenyl ether will guide the development of catalytic systems for aromatic C-O bond activation to achieve the highest possible selectivity and efficiency.

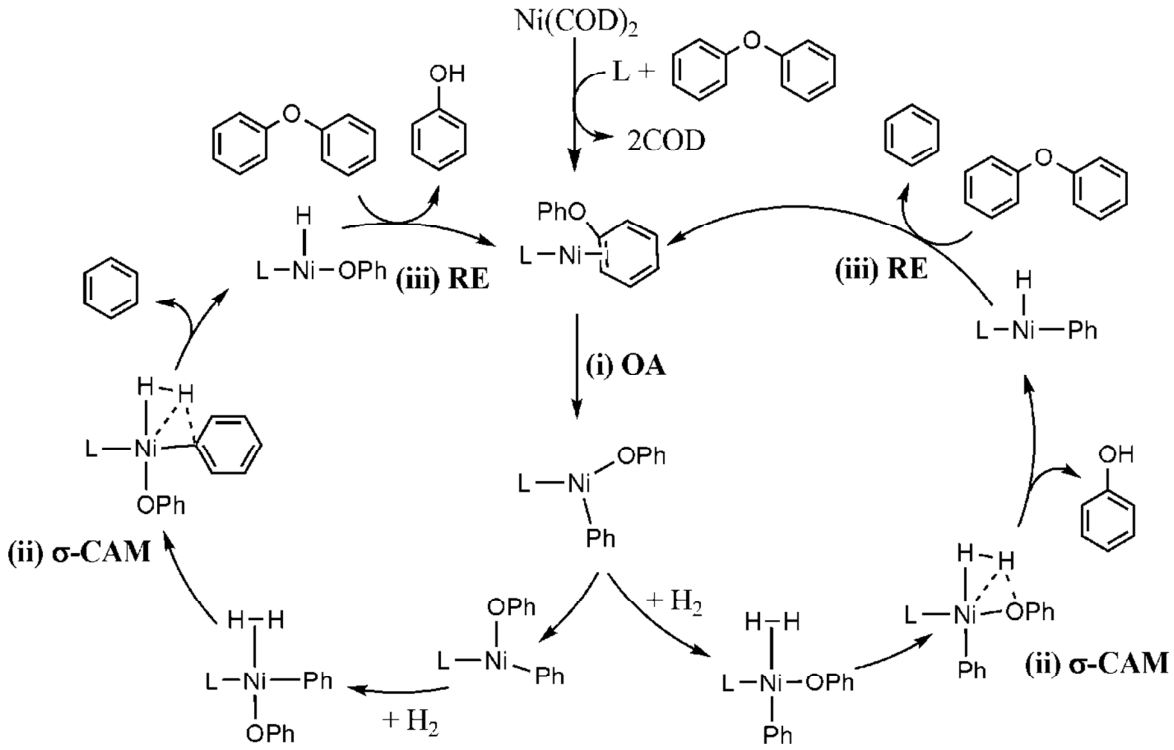

Scheme 2. Reaction mechanism for C-O bond hydrogenolysis of diphenyl ether by nickel *N*-heterocyclic carbene complex (L = SIPr). The catalytic cycle has three steps: (i) oxidative addition (OA), (ii) σ-complex-assisted metathesis (σ-CAM), and (iii) reductive elimination (RE).

COMPUTATIONAL DETAILS

All calculations were performed with Gaussian09 program.[14] All structures were fully optimized with default convergence criteria and frequencies were calculated to ensure that there was no imaginary frequency for minima and only one imaginary frequency corresponding to the reaction coordinate for transition states. The intrinsic reaction coordinate (IRC) calculations were performed to confirm that the transition states lead to the expected intermediates. Zero-point energies and thermodynamic functions were calculated at default settings (298.15 K and 1 atm). B3LYP[15-17] functional with basis set 1 (BS1) was used for all geometry optimizations and frequency calculations. In BS1, Stuttgart relativistic small core (RSC) 1997 ECP basis set[18] was used for Ni; 6-31++G(d,p)[19-21] was used for N, C, O, and H on the imidazole ring of SIPr (Scheme 1) and on the substrates, i.e., diphenyl ether and H_2; 6-31G[19-21] was used for all other atoms (the substituents on the imidazole ring

of SIPr). As M06[22] functional has been successfully used for other Ni complex studies,[23] we carried out single point energy and solvation free energy corrections by M06 with basis set 2 (BS2) on the gas-phase optimized structures using conductor-like polarizable continuum model (CPCM)[24, 25] with Bondi atomic radii and solvation parameters corresponding to *m*-xylene (ε = 2.348). BS2 is the same as BS1 except that 6-31G(d)[19-21] is used for the substituents on the imidazole ring of SIPr. The standard states were corrected to 1 mol/L.[26, 27] Unless otherwise specified, the energies mentioned throughout the article refer to relative free energies with solvent correction in *m*-xylene calculated by M06/BS2//B3LYP/BS1.

RESULTS AND DISCUSSION

A. Formation of the Ni(SIPr)(η^2-PhOPh) active species

Under the experimental conditions that Sergeev *et al.* reported,[2] *tert*-butoxide base was used to generate the free *N*-heterocyclic carbene ligand (SIPr) from SIPr·HCl. The cyclooctadiene (COD) in the $Ni(COD)_2$ precursor can easily undergo ligand substitution with SIPr to form Ni(SIPr)(COD) (-0.3 kcal/mol) (Fig. 1). From the X-ray crystal structure of (η^2;η^2-hexadiene)Ni(SIPr), two double bonds of hexadiene lie in the same coordination plane,[28] similarly for $(styrene)_2Ni(IPr)$.[29] Due to the ring constraint, two double bonds of COD cannot bind to the Ni in the same fashion as (hexadiene)Ni(SIPr) and $(styrene)_2Ni(IPr)$; only one of the double bonds of COD coordinates to the nickel in the calculated structure of Ni(SIPr)(COD) (Fig. S1).

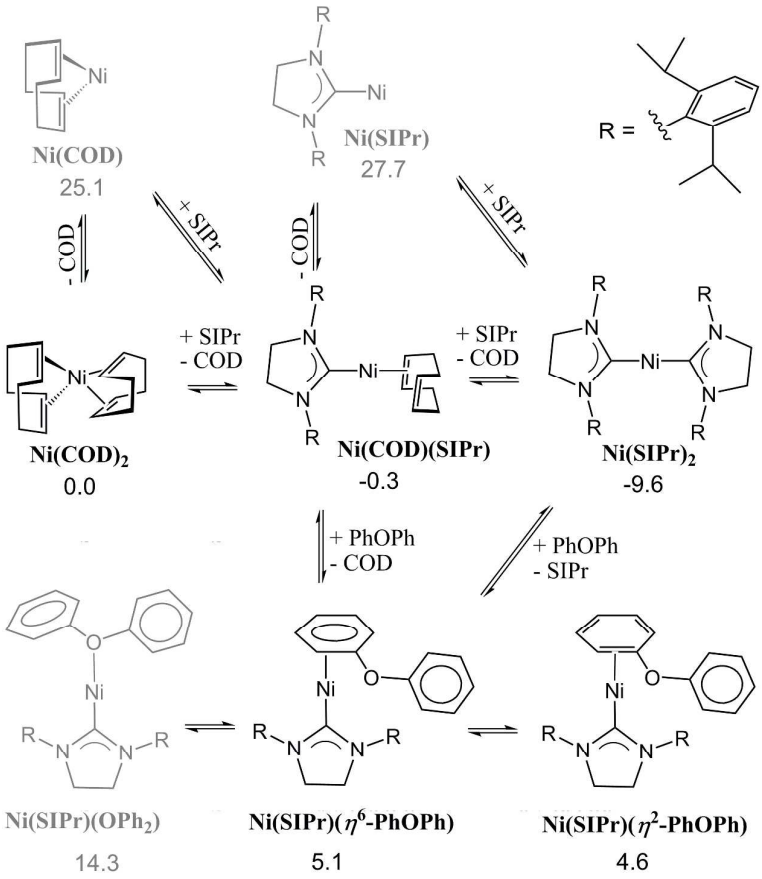

Fig. 1 Formation of Ni(SIPr)(η^2-PhOPh). The unfavorable species are shown in grey. Solvent corrected free energies relative to $Ni(COD)_2$ in *m*-xylene are given in kcal/mol.

While the ligand dissociation from Ni(SIPr)(COD) to form Ni(COD) and to form Ni(SIPr) is unfavorable (+25.1 and +27.7 kcal/mol, respectively) (Fig. 1), the ligand substitution of Ni(SIPr)(COD) with SIPr leads to the relatively stable $Ni(SIPr)_2$ complex (-9.6 kcal/mol). The calculated structure of $Ni(SIPr)_2$ is in good agreement with the X-ray crystal structure[30] (Fig. S2). Several studies on nickel phosphine[13, 31] and *N*-heterocyclic carbene (NHC)[32] complexes showed that for the sterically hindered mono-dentate ligands, the oxidative addition of the substrate preferably occurs on the mono-ligated complex rather than on the di-ligated complex. Here, we tried to locate $[Ni(SIPr)_2(Ph)(OPh)]^0$, the product of the oxidative addition of diphenyl ether on $Ni(SIPr)_2$, but all attempts were not successful. The oxidative addition of diphenyl ether on $Ni(SIPr)_2$ is unlikely due to the steric hindrance of SIPr.

Ogoshi and coworkers[33] reported that a mixture of $Ni(COD)_2$ and NHC (SIPr and IPr) in an arene solution under H_2 at room temperature led to the formation of Ni(NHC)(η^6-arene) complexes, as confirmed by X-ray crystal structures. According to their experiment,[33] the presence of H_2 under the reaction conditions essentially led to hydrogenation of cyclooctadiene to form cyclooctane, which cannot coordinate with Ni. As Sergeev *et al*. used similar experimental conditions,[2] the hydrogenation of cyclooctadiene is also expected. Although the COD substitution with diphenyl ether to form Ni(SIPr)(η^6-PhOPh) is slightly endergonic (+5.1 kcal/mol) (Fig. 1), the hydrogenation of COD should favor the formation of Ni(SIPr)(η^6-PhOPh). Moreover, Ni(SIPr)(η^6-PhOPh) is more favorable than Ni(SIPr)(η^6-*m*-xylene) by -7.2 kcal/mol (Fig. S3); thus, diphenyl ether can compete with *m*-xylene solvent to form the active species for C-O bond activation.

Other coordination modes of diphenyl ether to Ni were explored. The O-bound Ni(SIPr)(OPh_2) has a higher energy than η^6-bound Ni(SIPr)(η^6-PhOPh) (+9.2 kcal/mol) (Fig. 1), while Ni(SIPr)(η^2-PhOPh) has a similar energy to Ni(SIPr)(η^6-PhOPh) (-0.5 kcal/mol). Diphenyl ether in the η^6 and η^2 binding modes can accept a π-back donation from the electron rich Ni^0-SIPr. We propose that diphenyl ether is not only a substrate in the reaction but also serves as a ligand to stabilize the Ni-SIPr complex. Ni(SIPr)(η^6-PhOPh) can easily rearrange to Ni(SIPr)(η^2-PhOPh) (**IN1**), the active specie for C-O bond activation.

B. C-O bond hydrogenolysis

a) The oxidative addition

The Ni(SIPr)(η^2-PhOPh) (**IN1**) complex undergoes oxidative addition to form transition state **TS1**, which has a three-centered interaction and an energy barrier of +24.0 kcal/mol, leading to formation of $[Ni^{II}(SIPr)(Ph)(OPh)]^0$ (**IN2**) (Fig.2). The three-coordinate complex, **IN2**, with the phenyl group *trans* to the vacant site, can rearrange to **IN3** and **IN4**, with the phenolate and the SIPr *trans* to the vacant site, respectively (Fig. S4). The phenolate in **IN4** is actually in an η^3-coordination; the Ni-O bond distance is 1.93 Å, the Ni-C^{ipso} bond distance is 2.23 Å, and the Ni-C^{ortho} bond distance is 2.33 Å. These bond distances are similar to those in the crystal structure of the Ni *o*-methylbenzyl

η^3-complex.[34] Accordingly, **IN4** is the most stable structure. Note that there is no agostic or anagostic[35] interaction in either **IN2** or **IN3**; the distance between the isopropyl CH on the substituent of SIPr and the Ni is >3.0 Å (Fig. S4). As two strong *trans* influence ligands (phenyl and SIPr) are located in the opposite positions of the Ni, the Ni-C(SIPr) bond distance in **IN3** is 2.03 Å, relatively weaker than the corresponding bond in **IN2** (~1.88 Å). Thus, **IN3** is less stable than **IN2**.

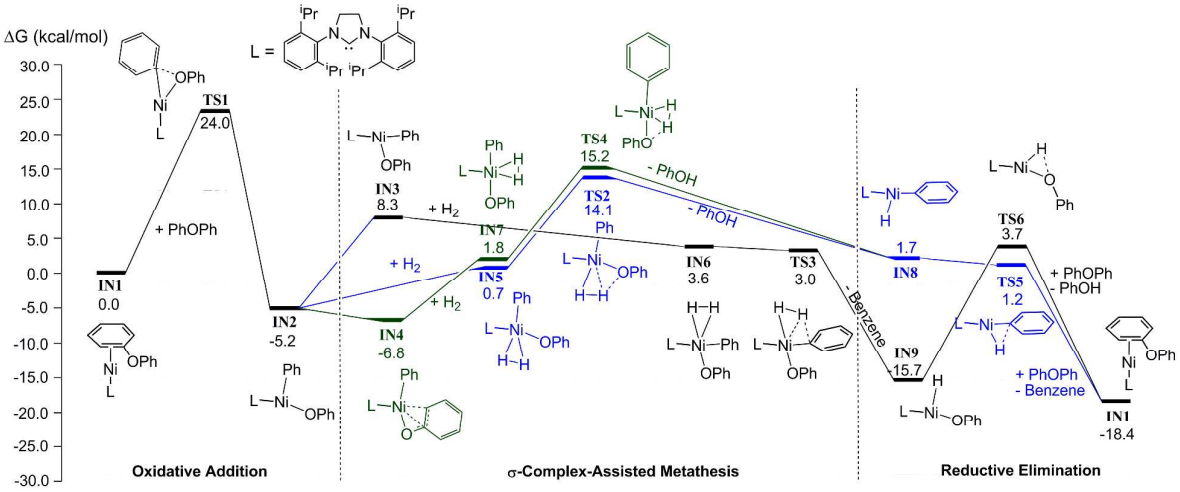

Fig. 2 Relative free energy profiles for the overall mechanism for the C-O bond hydrogenolysis of diphenyl ether. Solvent corrected relative free energies in *m*-xylene are given in kcal/mol.

The binding of H_2 to **IN1** to form the H_2-complex, Ni(SIPr)(η^2-PhOPh)(H_2) (Fig. S9) was also investigated. Generally, the dihydride mononuclear Ni complex is unstable,[36] while the H_2 adducts of Ni complexes are observable and can undergo heterolytic cleavage assisted by an amine base.[37, 38] The nickel hydride pathway should involve *tert*-butoxide in abstracting a proton from Ni(SIPr)(η^2-PhOPh)(H_2) to generate the nickel hydride species. Thus, we investigated the deprotonation of Ni(SIPr)(η^2-PhOPh)(H_2) by *tert*-butoxide base. However, steric hindrance from the ligands around the Ni atom prevented *tert*-butoxide access to abstract the proton. To the best of our knowledge, currently there is no experimental support for the formation of nickel hydride intermediates under these reaction conditions. Therefore, we exclude the nickel hydride pathway in this study.

b) The σ-Complex-Assisted Metathesis (σ-CAM)

As some Ni(II) complexes were found in the triplet state,[39-41] we explored the triplet complex, $[Ni^{II}(SIPr)(Ph)(OPh)]^0$ (**IN2$_T$**) (Fig. S5). While the singlet complexes (**IN2**, **IN3**, and **IN4**) have T-shaped structures, the triplet **IN2$_T$** structure is a tetrahedron with a missing cap (Fig. S5).[41] Two singly occupied molecular orbitals are Ni d_{x2-y2}-based and Ni d_{xy}-based orbitals with antibonding character (Fig. S6). Although the energy of **IN2$_T$** is only 2.8 kcal/mol higher than that of **IN2** (Fig. S5), the triplet Ni(II) H_2-complex could not be located. Upon geometry optimization, the H_2 simply dissociated away from the Ni. In the [NiFe] hydrogenase model study, Keith and Hall also reported that while the triplet state was possible for the Ni(II), H_2 binding to the high spin Ni was not found.[42] Since the triplet complex is unlikely to bind H_2 and to undergo hydrogenolysis, only singlet complexes are discussed in this study.

For complexes **IN2**-**IN4**, the LUMO is a Ni d_{x2-y2}-based orbital with σ-antibonding character (Fig.S7). As phenolate, the weak σ-donor ligand, is opposite to the vacant site, **IN3** has the lowest LUMO energy (Scheme 3). The HOMO of **IN3** is a Ni d_{xy}-based orbital with π-antibonding to the oxygen p_y-orbital of OPh (Fig.S7). In contrast, for the HOMO of **IN4**, not only does the Ni d_{xy} orbital have a π-antibonding interaction with the π-orbital of phenyl, but it also has a bonding interaction with the π-orbital of OPh at one of the *ortho* carbons (Fig.S7). Thus, the HOMO energy of **IN4** is lower than that of **IN3**, making it more stable than **IN3**. Since the binding of H_2 at the vacant site of $[Ni^{II}(SIPr)(Ph)(OPh)]^0$ involves a charge transfer from the HOMO to the σ*-orbital of H_2 and a charge transfer from the σ-orbital of H_2 to the LUMO (Scheme 4), the highest HOMO energy and the lowest LUMO energy in **IN3** (Scheme 3) should facilitate the binding of H_2 to **IN3**. Correspondingly, **IN3** readily binds H_2 at the vacant site (-4.7 kcal/mol), while the binding of H_2 on **IN4** and **IN2** are unfavorable (~ 6-8 kcal/mol) (Fig. 2).

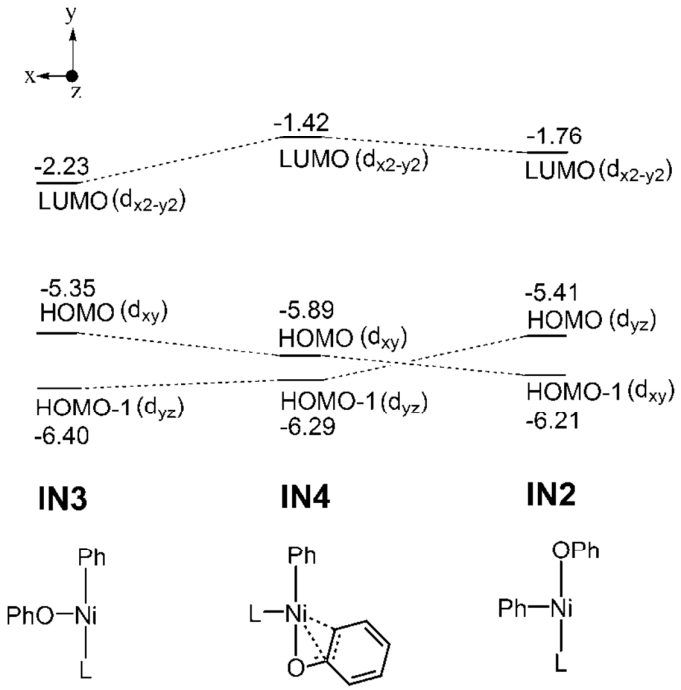

Scheme 3. Selected molecular orbital energies (in eV) for **IN3**, **IN4** and **IN2**.

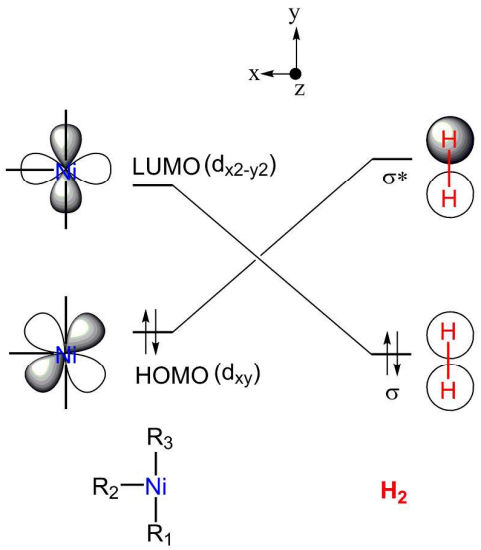

Scheme 4. H_2 orbital interaction with the d_{x2-y2}-based and the d_{xy}-based orbitals of the three-coordinate Ni(II) complex.

The binding of H_2 at the vacant site of $[Ni(SIPr)(Ph)(OPh)]^0$ (**IN2**, **IN3**, and **IN4**) leads to the formation of the H_2-complex $[Ni(H_2)(SIPr)(Ph)(OPh)]^0$ (**IN5**, **IN6**, and **IN7**, respectively) (Fig.2). Generally, dihydride complexes can be formed on the electron rich transition metal, which can

provide a π-backbonding to the binding H_2.[43-45] Here the dihydride complex, $[Ni(H)(H)(SIPr)(Ph)(OPh)]^0$, the product from the oxidative addition of H_2 on $[Ni^{II}(SIPr)(Ph)(OPh)]^0$ was not found. Therefore, the H_2-complex $[Ni(H_2)(SIPr)(Ph)(OPh)]^0$ undergoes O-H bond and C-H bond formation through σ-bond metathesis.

IN5 can proceed to the σ-bond metathesis *via* the transition state **TS2**, which involves a four-centered interaction (Fig.3). Although the H_2 is perpendicular to the coordination plane of **IN5** (Fig.3), the rotational barrier for H_2 is rather small (1-2 kcal/mol).[46] The geometry of **TS2** has the transferred H close to Ni (1.72 Å); this can be classified as σ-complex-assisted metathesis (σ-CAM) as suggested for late transition metal complexes.[47, 48] The O-H bond is formed and the H-H bond is weakened. The T-shaped nickel complex $[Ni(SIPr)(Ph)(H)]^0$ with the hydride *trans* to the empty site (**IN8**) is then obtained, and phenol is eliminated. The overall energy barrier is +19.3 kcal/mol (Fig. 2). Similarly, **IN7** can undergo σ-complex-assisted metathesis *via* **TS4** to form the O-H bond (Fig. 3), leading to **IN8** formation and phenol elimination. The overall energy barrier (+22.0 kcal/mol) is slightly higher than that *via* **TS2** (Fig. 2).

On the other hand, σ-CAM *via* **IN6** and transition state **TS3** is facile (Fig. 2). The electronic energy of **TS3** is slightly higher than that of **IN6** (Table S1). After the solvent correction, the free energy of **TS3** becomes slightly lower than **IN6** (< 1 kcal/mol) (Fig. 2). The intrinsic reaction coordinate (IRC) calculations indicated that **TS3** really is the transition state for the σ-CAM of **IN6**. The nickel assists with the H-H bond cleavage and the C-H bond formation; the T-shaped nickel complex $[Ni(SIPr)(OPh)(H)]^0$ with the hydride *trans* to the empty site (**IN9**) and benzene are obtained as products. The benzene elimination is more favorable than the phenol elimination by -17.4 kcal/mol (Fig. 2), corresponding to the stronger C-H bond in comparison to the O-H bond.[49]

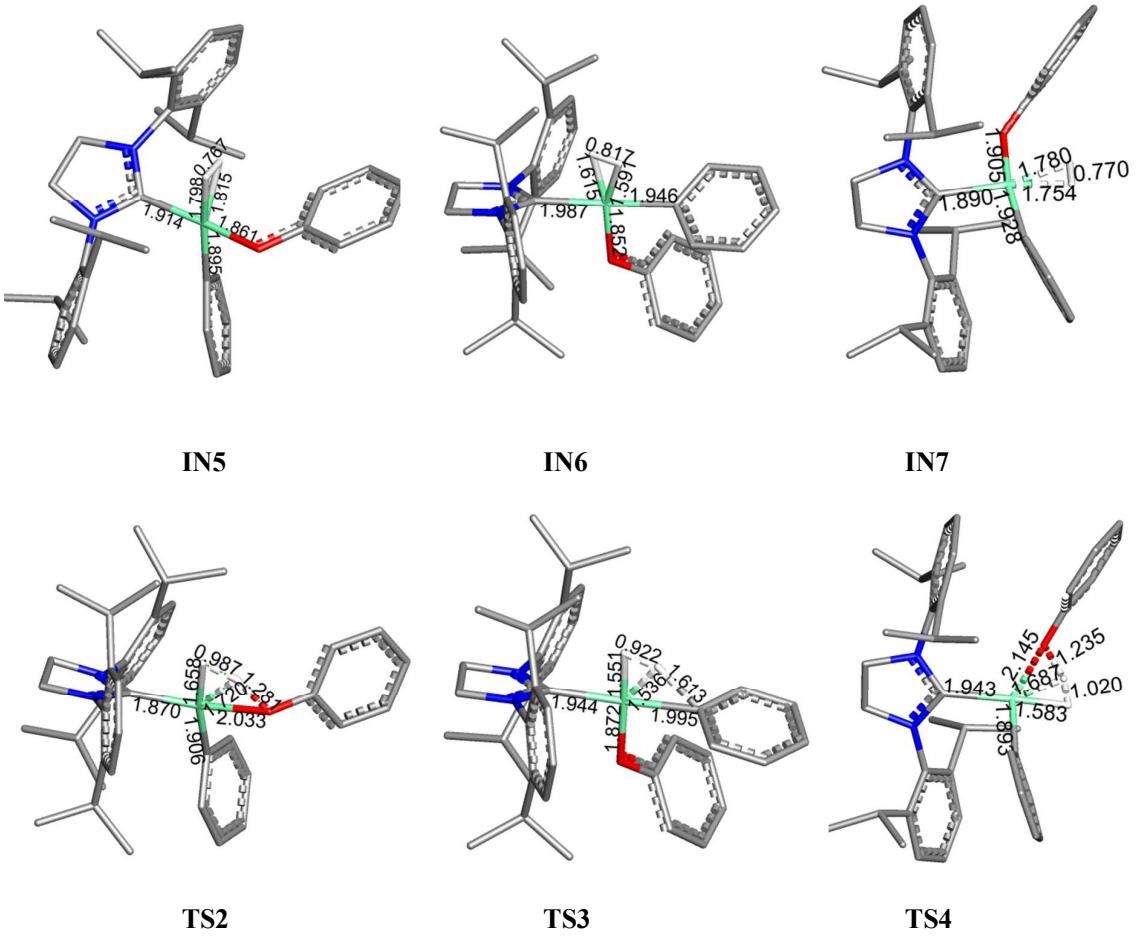

Fig. 3 Optimized geometries of σ-CAM intermediates $[Ni(H_2)(SIPr)(Ph)(OPh)]^0$ (**IN5**, **IN6**, and **IN7**) and transition states (**TS2**, **TS3**, and **TS4**). Calculated bond distances are shown in Å. All H atoms are omitted for clarity except for those of H_2. Ni atoms are shown in green, C atoms in grey, O atoms in red, N atoms in blue, and H atoms in white.

Note that the energy barrier for the H_2 addition across the Ni-Ph bond *via* **IN6** is lower than that across the Ni-OPh bond *via* **IN5** and **IN7**. This can be related to the structural change upon σ-CAM. With H_2 opposite to the weak *trans* ligand, **IN6** has stronger Ni-H bonds (~1.6 Å) than those on **IN5** and **IN7** (~1.8 Å) (Fig. 3). The H-H bond on **IN6** (0.82 Å) is also weaker than those on **IN5** and **IN7** (0.77-0.78 Å). These should facilitate the H-H bond cleavage in **IN6**. Moreover, the geometry of **TS3** is only slightly changed from that of **IN6**; the H-H distance is lengthened by ~0.1 Å and the Ni-Ph distance is slightly lengthened (0.05 Å) (Fig. 3). On the other hand, the changes in geometries from **IN5** to **TS2** and from **IN7** to **TS4** are more pronounced; the H-H distances and the Ni-OPh distances

are lengthened by ~0.2 Å. Thus, the energy barrier for the O-H bond formation is higher than that for the C-H bond formation (Fig. 2).

c) The Reductive Elimination

IN8 readily proceeds to reductive elimination of benzene *via* a three-centered transition state, **TS5** (Fig. 2). Diphenyl ether then binds to the Ni to regenerate Ni(SIPr)(η^2-PhOPh). The C-H distance in **IN8** is shortened by -0.65 Å to form a bond in **TS5** (Fig. 4). On the other hand, **IN9** undergoes reductive elimination *via* **TS6** to generate phenol with a high energy barrier of +19.4 kcal/mol. The O-H distance in **IN9** is shortened by -1.27 Å to form a bond in **TS6**. Corresponding to the energy barriers, the structure of **TS5** represents the "earlier" transition state compared to that of **TS6** (Fig.4).

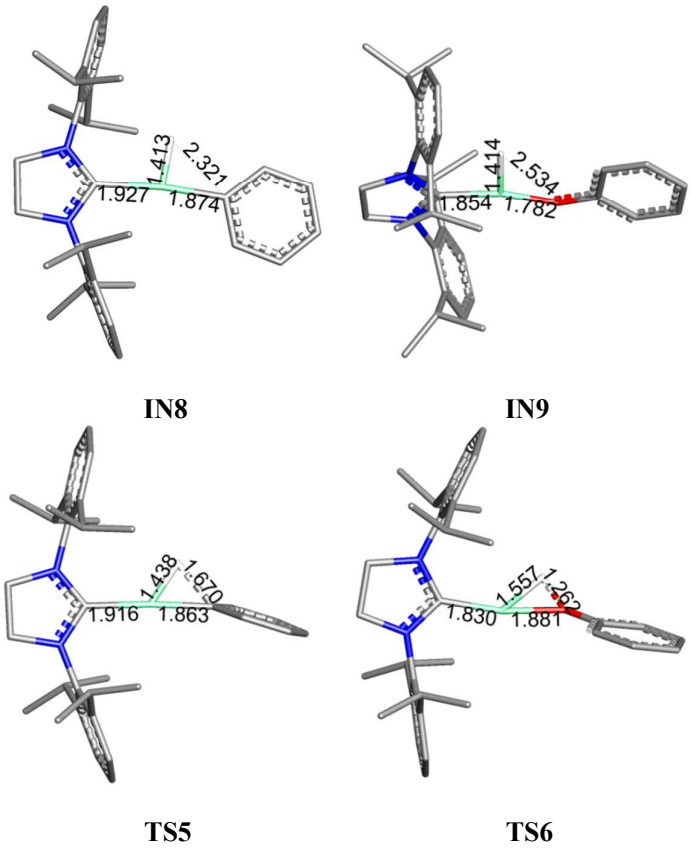

Fig. 4 Optimized geometries of reductive elimination intermediates (**IN8** and **IN9**) and transition states (**TS5** and **TS6**). Calculated bond distances are shown in Å. All H atoms are omitted for clarity except for the one on Ni. Ni atoms are shown in green, C atoms in grey, O atoms in red, N atoms in blue, and H atoms in white.

The possibility of four-coordinate intermediates for the reductive elimination was also investigated. The binding of diphenyl ether to **IN9** was calculated. The O-bound square planar complex, Ni(SIPr)(H)(OPh)(OPh_2), can be formed with an increase in energy of 3.5 kcal/mol (Fig. S8) while the η^2- and η^6-bound complexes were not found. The Ni-OPh_2 distance in Ni(SIPr)(H)(OPh)(OPh_2) is rather long (2.44 Å). Moreover, the transition state for the reductive elimination of phenol cannot be located; diphenyl ether dissociated away and the structure became **TS6** during the transition state optimization. Thus, it is unlikely that the diphenyl ether coordinates to Ni^{II}(SIPr)(H)(OPh), **IN9**, before the reductive elimination of phenol.

d) The Overall Mechanism

In the mixture of SIPr, diphenyl ether, and H_2, the $Ni(COD)_2$ precursor can form Ni(SIPr)(η^6-PhOPh), which can readily rearrange to Ni(SIPr)(η^2-PhOPh) (**IN1**). The Ni(SIPr)(η^2-PhOPh) complex undergoes oxidative addition to form $[Ni(SIPr)(Ph)(OPh)]^0$ with an energy barrier of +24.0 kcal/mol (Fig.2). Considering the overall catalytic reaction, this is the rate determining step. Then, **IN2**, the $[Ni(SIPr)(Ph)(OPh)]^0$ complex with the phenyl *trans* to the vacant site is formed. **IN2** can rearrange to **IN3**, the $[Ni(SIPr)(Ph)(OPh)]^0$ complex with the phenolate *trans* to the vacant site. **IN3** can then bind H_2, proceed to σ-complex-assisted metathesis to generate benzene, and reductively eliminate phenol with the highest energy barrier at the reductive elimination step (+19.4 kcal/mol). Alternatively, **IN2** can bind H_2, proceed to σ-complex-assisted metathesis to generate phenol, and reductively eliminate benzene with the highest energy barrier at the σ-CAM step (+19.3 kcal/mol). The energy barriers for the pathway *via* **IN3** and *via* **IN2** are comparable; thus, both pathways are possible. Notably, for both pathways, C-H bond formation is facile, while O-H bond formation requires more structural changes and needs to overcome a high energy barrier (~19 kcal/mol).

From the experiment by Sergeev and Hartwig,[2] a large amount of $Ni(COD)_2$ precursor and SIPr ligand (10-20%) was used to complete the reaction at 100-120 ^oC. This supports the formation and accumulation of $Ni(SIPr)_2$, which is not the key species for C-O bond activation. Although the formation of Ni(SIPr)(η^2-PhOPh), the active species, is feasible, the Ni(SIPr)(η^2-PhOPh) is less stable than $Ni(SIPr)_2$ (~14 kcal/mol) (Fig. 1). In place of the formation of the catalyst *in situ* from $Ni(COD)_2$,

SIPr·HCl, and ^{t}BuO^{-} base, Ni(SIPr)(η^6-arene) could be worth exploring as a starting catalyst. Since the Ni:SIPr ratio is kept at 1:1, the redistribution of Ni(SIPr)(η^6-arene) to Ni(SIPr)$_2$ should be minimal. According to our study, the Ni(SIPr)(η^6-arene) can readily rearrange to Ni(SIPr)(η^2-PhOPh), the active species for the C-O bond activation. The synthesis of Ni(SIPr)(η^6-arene) is known as recently reported by Ogoshi and coworkers.[33]

C. C-O Bond Activation Selectivity

Since the oxidative addition step was found to be the rate determining step, we also investigated the oxidative addition of diaryl ethers, which contain the electron withdrawing trifluoromethyl group. The Ni(SIPr)(η^2-$C_6H_4CF_3OPh$) complex with η^2-coordination at the aryl ring, in which the trifluoromethyl group is located (**IN1-Fa**), is slightly more stable than the complex with η^2-coordination at the phenyl ring (**IN1-Fb**) (-1.04 kcal/mol) (Fig. 5); correspondingly, the Ni-C(aryl) bond distances on **IN1-Fa** are slightly shorter than those on **IN1-Fb** and **IN1** (Fig. 6).

C-O bond activation preferably occurs at the carbon on the aryl ring with the trifluoromethyl group *via* **TS1-Fa** (+21.6 kcal/mol) rather than on the unsubstituted aryl ring *via* **TS1-Fb** (+25.3 kcal/mol); the Ni-C^{ipso} bond distance on **TS1-Fa** is lengthened from that on **IN1-Fa** by 0.03 Å while that on **TS1-Fb** is lengthened by 0.04 Å (Fig. 6). Thus, the former reaction, which leads to phenol and $C_6H_5CF_3$ as products, is more favorable, in agreement with the products observed experimentally.[2] The free energy barrier for the oxidative addition of Ni(SIPr)(η^2-$C_6H_4CF_3OPh$) *via* **TS1-Fa** is also lower than that of Ni(SIPr)(η^2-PhOPh) *via* **TS1** (+24.0 kcal/mol); correspondingly, Sergeev *et al*. showed that the reaction of the diaryl ether containing a trifluoromethyl substituent can proceed at a lower temperature than that of diphenyl ether.[2] Similar to the study on the oxidative addition of substituted aryl halide on palladium[50] and rhodium[51] complexes, the electron withdrawing group on the aryl ring accelerates the oxidative addition reaction.

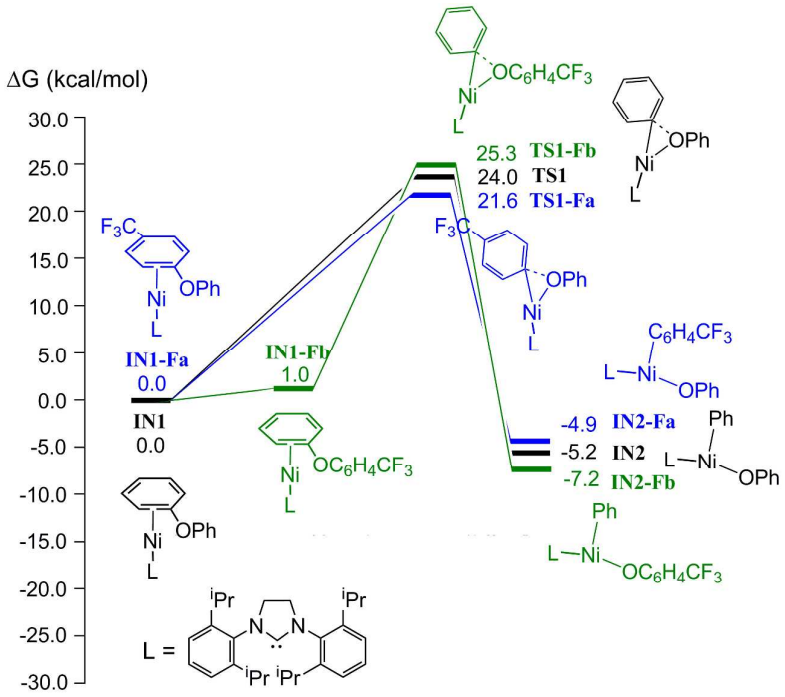

Fig. 5 Free energy profiles for the oxidative addition of diaryl ether. Solvent corrected relative free energies in *m*-xylene are given in kcal/mol.

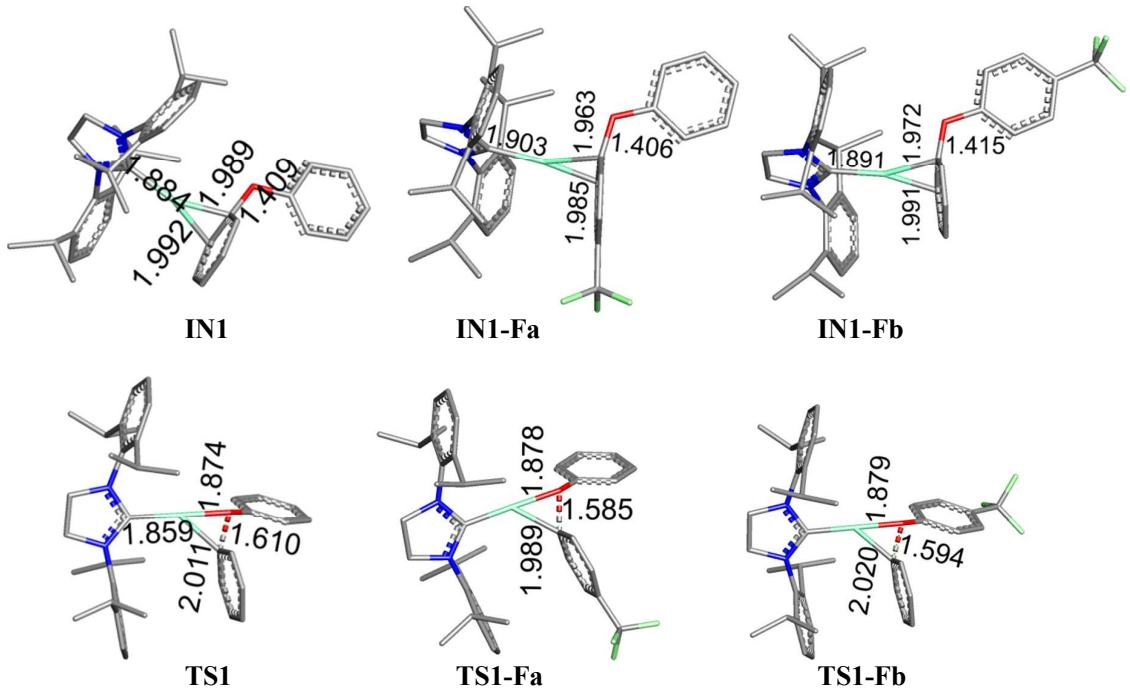

Fig.6 Optimized geometries in the oxidative addition of Ni(SIPr)(η^2-PhOPh) and the oxidative addition of Ni(SIPr)(η^2-$C_6H_4CF_3OPh$).

D. Hydrogenation

Unlike for the heterogeneous Ni catalysts, the hydrogenation products, e.g., cyclohexadiene and cyclohexane, were not observed for the Ni-SIPr catalytic system.[2] As the structure of Ni(NHC)(benzene) is known,[33] the formation of Ni(SIPr)(η^6-C_6H_6) is expected. Our calculation also shows that the ligand exchange of diphenyl ether with benzene in Ni(SIPr)(η^6-PhOPh) is favorable; the Ni(SIPr)(η^6-C_6H_6) is slightly more stable than Ni(SIPr)(η^6-PhOPh) (-1.2 kcal/mol) (Fig. S3). While the Ni(SIPr)(η^6-PhOPh) can readily transform to Ni(SIPr)(η^2-PhOPh) (Fig. 1), the same occurs for Ni(SIPr)(η^6-C_6H_6) to Ni(SIPr)(η^2-C_6H_6) (Fig. 7). Thus, we investigated the hydrogenation of Ni(SIPr)(η^2-C_6H_6).

The binding of H_2 to Ni(SIPr)(η^2-C_6H_6) (**IN10**) leads to the formation of the H_2-complex, [Ni^0(SIPr)(H_2)(η^2-C_6H_6)] (**IN11**) with a H-H distance of 0.83 Å (Fig. 8); the reaction is unfavorable with a change in the free energy of +6.5 kcal/mol (Fig.7). The H-transfer from the Ni to the adjacent carbon on the benzene then occurs *via* the transition state **TS7** with an overall energy barrier of +25.1 kcal/mol. On **TS7**, the breaking H-H bond distance is lengthened by +0.84 Å and the forming C-H bond distance is shortened by -0.92 Å from those on **IN11**. The C-H bond is completely formed in **IN12** (1.25 Å) (Fig. 8). There is a C-H agostic interaction in **IN12** (with the Ni-H distance of 1.58 Å), similar to Spencer's β-agostic nickel ethyl cations (with the Ni-H distance of 1.64 Å).[52, 53] **IN12** is almost isoenergetic (< 1 kcal/mol) to **TS7**.

The reductive elimination of cyclohexadiene from **IN12** involves the three-centered transition state, **TS8** with a rather high overall energy barrier of +39.0 kcal/mol, leading to the formation of [Ni^0(SIPr)(η^2-C_6H_8)] (**IN13**). Moreover, the overall process is endergonic (+7.2 kcal/mol) (Fig. 7). Therefore, the formation of cyclohexadiene and other hydrogenation products are unlikely to occur. This corresponds to the experimental results[2] that reported only benzene and phenol as products.

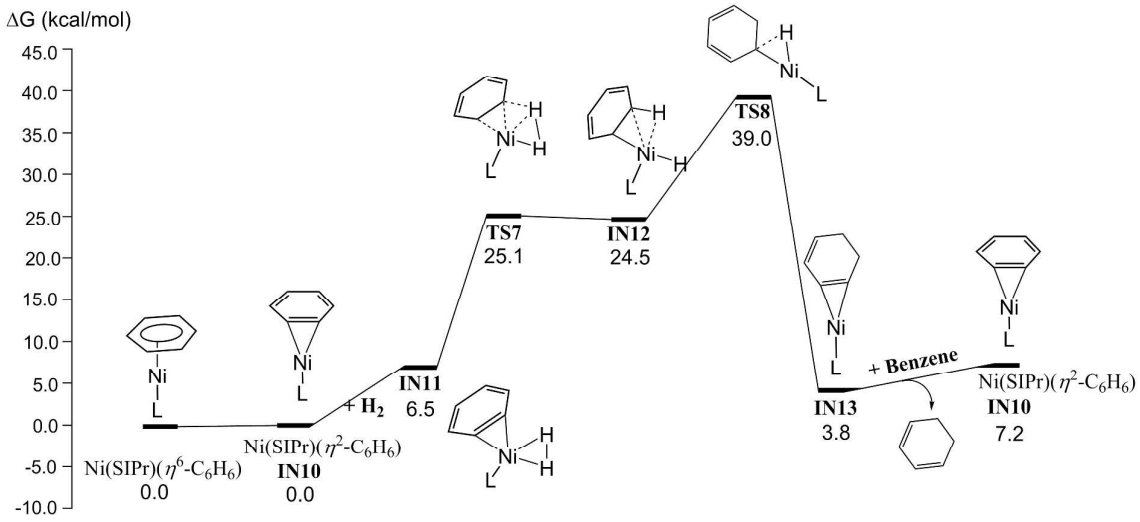

Fig.7 Free energy profiles for the hydrogenation of benzene. Solvent corrected relative free energies in *m*-xylene are given in kcal/mol.

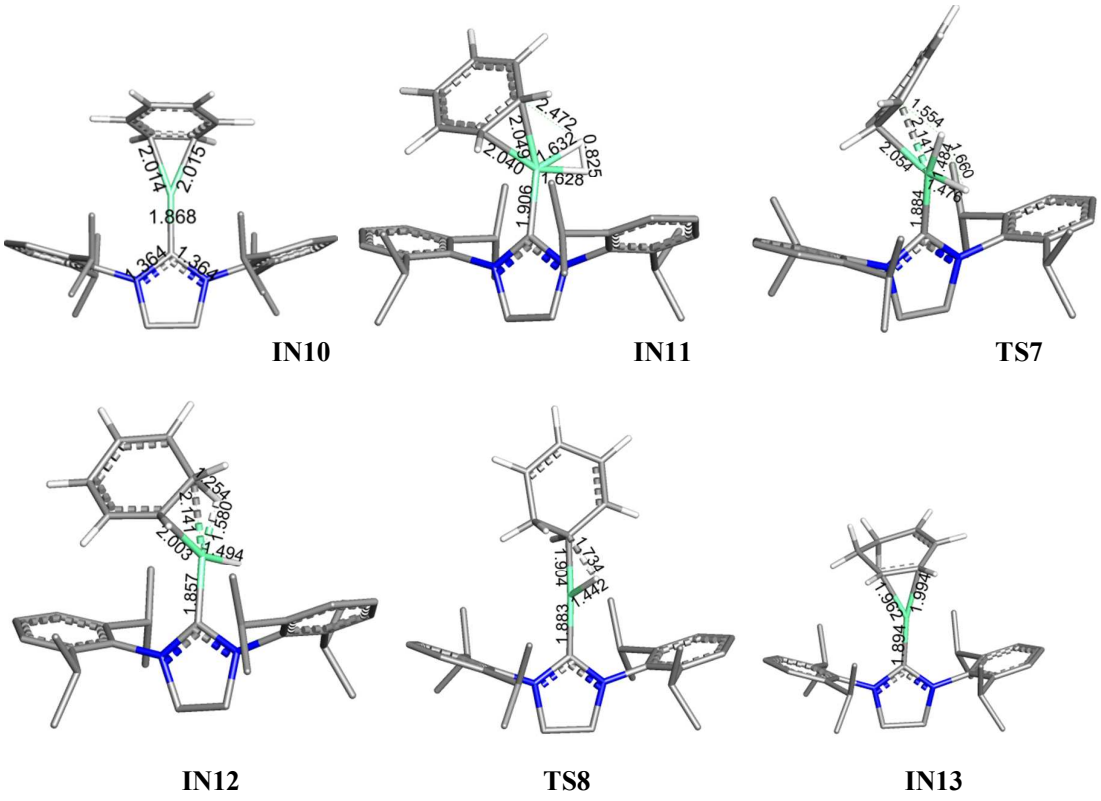

Fig.8 Optimized structures for the hydrogenation of benzene on Ni-SIPr. Calculated bond distances are shown in Å.

CONCLUSIONS

We investigated the mechanisms for the C-O bond hydrogenolysis of diphenyl ether by the nickel *N*-heterocyclic carbene (Ni-SIPr) complex to obtain benzene and phenol as products. According to the calculations, the $Ni(COD)_2$ precursor can undergo ligand substitutions with SIPr and with diphenyl ether to form Ni(SIPr)(η^6-PhOPh). The Ni(SIPr)(η^6-PhOPh) complex can readily rearrange to Ni(SIPr)(η^2-PhOPh), the active species for C-O bond activation. Thus, diphenyl ether is not only a substrate, but also serves as a ligand to stabilize the Ni-SIPr complex. Although the formation of Ni(SIPr)(η^2-PhOPh), the active species, is feasible, the Ni(SIPr)(η^2-PhOPh) complex is less stable than $Ni(SIPr)_2$, the catalytically inactive species. To minimize the formation and accumulation of $Ni(SIPr)_2$, we suggest that Ni(SIPr)(η^6-arene) should be explored as a starting catalyst. The synthesis of Ni(SIPr)(η^6-arene) is known and Ni(SIPr)(η^6-arene) can easily undergo ligand exchange with diphenyl ether to form Ni(SIPr)(η^2-PhOPh).

The catalytic reaction has three steps: (i) oxidative addition of Ni(SIPr)(η^2-PhOPh) to form $[Ni(SIPr)(OPh)(Ph)]^0$, (ii) σ-complex-assisted metathesis (σ-CAM), in which H_2 binds to Ni to form $[Ni(SIPr)(OPh)(Ph)(H_2)]^0$, then benzene (or phenol) is eliminated, and (iii) reductive elimination of phenol (or benzene) and rebinding of diphenyl ether to regenerate Ni(SIPr)(η^2-PhOPh). The rate determining step was found to be the oxidative addition step (+24 kcal/mol), in agreement with the experimental results which showed that the substrate with an electron withdrawing substituent on the aryl ring can undergo the catalytic reaction for C-O bond hydrogenolysis at a lower temperature than the unsubstituted aryl ether. We also revealed that the hydrogenation of benzene *via* Ni(SIPr)(η^2-C_6H_6) requires a high energy barrier (+39.0 kcal/mol), corresponding to the experimental results in that the hydrogenation products, e.g., cyclohexane, cyclohexadiene, were not observed. Understanding the reaction mechanisms of the nickel catalysts for C-O bond hydrogenolysis of diphenyl ether will provide useful guidance for the development of catalytic systems to achieve the highest possible selectivity and efficiency in aromatic C-O bond activation. The selectivity towards the C-O bond activation at the aromatic C-O bond over the aliphatic C-O bond is under investigation.

ACKNOWLEDGMENTS

Financial supports from the Thailand Research Fund (Grant No. MRG5580117 and TRG5780286), Development and Promotion of Science and Technology Talents Project (DPST) (Grant No. 025/2555), the Center of Excellence for Innovation in Chemistry (PERCH-CIC), Office of the Higher Education Commission (CHE), and Ministry of Education are gratefully acknowledged. This research project is supported by Faculty of Science, Mahidol University.

NOTES AND REFERENCES

Electronic Supplementary Information (ESI) available: Fig.s (energies and graphical representations) and xyz coordinates. See DOI: 10.1039/b000000x/

1. J. Zakzeski, P. C. A. Bruijnincx, A. L. Jongerius and B. M. Weckhuysen, *Chem. Rev.*, 2010, **110**, 3552-3599.
2. A. G. Sergeev and J. F. Hartwig, *Science*, 2011, **332**, 439-443.
3. E. Wenkert, E. L. Michelotti and C. S. Swindell, *J. Am. Chem. Soc.*, 1979, **101**, 2246-2247.
4. B.-J. Li, L. Xu, Z.-H. Wu, B.-T. Guan, C.-L. Sun, B.-Q. Wang and Z.-J. Shi, *J. Am. Chem. Soc.*, 2009, **131**, 14656-14657.
5. B.-T. Guan, S.-K. Xiang, B.-Q. Wang, Z.-P. Sun, Y. Wang, K.-Q. Zhao and Z.-J. Shi, *J. Am. Chem. Soc.*, 2008, **130**, 3268-3269.
6. B.-J. Li, Y.-Z. Li, X.-Y. Lu, J. Liu, B.-T. Guan and Z.-J. Shi, *Angew. Chem., Int. Ed.*, 2008, **47**, 10124-10127.
7. B.-T. Guan, Y. Wang, B.-J. Li, D.-G. Yu and Z.-J. Shi, *J. Am. Chem. Soc.*, 2008, **130**, 14468-14470.
8. M. Tobisu, T. Shimasaki and N. Chatani, *Angew. Chem., Int. Ed.*, 2008, **47**, 4866-4869.
9. G. A. Molander and F. Beaumard, *Org. Lett.*, 2010, **12**, 4022-4025.
10. J. He, C. Zhao and J. A. Lercher, *J. Am. Chem. Soc.*, 2012, **134**, 20768-20775.
11. J. Choi, Y. Choliy, X. Zhang, T. J. Emge, K. Krogh-Jespersen and A. S. Goldman, *J. Am. Chem. Soc.*, 2009, **131**, 15627-15629.
12. Z. Li, Y. Y. Jiang and Y. Fu, *Chemistry*, 2012, **18**, 4345-4357.
13. Z. Li, S.-L. Zhang, Y. Fu, Q.-X. Guo and L. Liu, *J. Am. Chem. Soc.*, 2009, **131**, 8815-8823.
14. G. W. T. M. J. Frisch, H. B. Schlegel, G. E. Scuseria,, J. R. C. M. A. Robb, G. Scalmani, V. Barone, B. Mennucci,, H. N. G. A. Petersson, M. Caricato, X. Li, H. P. Hratchian,, J. B. A. F. Izmaylov, G. Zheng, J. L. Sonnenberg, M. Hada,, K. T. M. Ehara, R. Fukuda, J. Hasegawa, M. Ishida, T. Nakajima,, O. K. Y. Honda, H. Nakai, T. Vreven, J. A. Montgomery, Jr.,, F. O. J. E. Peralta, M. Bearpark, J. J. Heyd, E. Brothers,, V. N. S. K. N. Kudin, T. Keith, R. Kobayashi, J. Normand,, A. R. K. Raghavachari, J. C. Burant, S. S. Iyengar, J. Tomasi,, N. R. M. Cossi, J. M. Millam, M. Klene, J. E. Knox, J. B. Cross,, C. A. V. Bakken, J. Jaramillo, R. Gomperts, R. E. Stratmann,, A. J. A. O. Yazyev, R. Cammi, C. Pomelli, J. W. Ochterski,, K. M. R. L. Martin, V. G. Zakrzewski, G. A. Voth,, J. J. D. P. Salvador, S. Dapprich, A. D. Daniels, and J. B. F. O. Farkas, J. V. Ortiz, J. Cioslowski, D. J. Fox, *Gaussian 09, Revision C.01, Gaussian, Inc., Wallingford CT*, 2010.
15. A. D. Becke, *J. Chem. Phys.* , 1993, **98**, 5648.
16. C. Lee, W. Yang and R. G. Parr, *Phys. Rev. B* 1988, **37**, 785.
17. P. J. Stephens, F. J. Devlin, C. F. Chabalowski and M. J. Frisch, *J. Phys. Chem.*, 1994, **98**, 11623.

18. A. Bergner, M. Dolg, W. Kuumlchle, H. Stoll and H. Preuszlig, *Mol. Phys.*, 1993, **80**, 1431.
19. P. C. Hariharan and J. A. Pople, *Theor. Chim. Acta* 1973, **28**, 213-222.
20. G. A. Petersson and M. A. Al-Laham, *J. Chem. Phys.* , 1991 **94**, 6081-6090.
21. G. A. Petersson, A. Bennett, T. G. Tensfeldt, M. A. Al-Laham, W. A. Shirley and J. Mantzaris, *J. Chem. Phys.* , 1988, **89**, 2193-2218.
22. Y. Zhao and D. G. Truhlar, *Theor. Chem. Acc.* , 2008, **120**, 215.
23. J. Cornella, E. Gómez-Bengoa and R. Martin, *J. Am. Chem. Soc.*, 2013, **135**, 1997–2009.
24. V. Barone and M. Cossi, *J. Phys. Chem. A* 1998, **102**, 1995.
25. M. Cossi, N. Rega, G. Scalmani and V. Barone, *J. Comp. Chem.* , 2003, **24**, 669-681.
26. P. Surawatanawong, Y. Fan and M. B. Hall, *J. Organomet. Chem.*, 2008, **693**, 1552-1563.
27. C. J. Cramer, *Essentials of Computational Chemistry: Theories and Models*, Wiley, 2004.
28. J. Wu, J. W. Faller, N. Hazari and T. J. Schmeier, *Organometallics*, 2012, **31**, 806-809.
29. M. J. Iglesias, J. F. Blandez, M. R. Fructos, A. Prieto, E. Álvarez, T. R. Belderrain and M. C. Nicasio, *Organometallics*, 2012, **31**, 6312-6316.
30. A. A. Danopoulos and D. Pugh, *Dalton Trans.*, 2008, 30-31.
31. X. Hong, Y. Liang and K. N. Houk, *J. Am. Chem. Soc.*, 2014, **136**, 2017-2025.
32. V. P. W. Böhm, C. W. K. Gstöttmayr, T. Weskamp and W. A. Herrmann, *Angew. Chem., Int. Ed.*, 2001, **40**, 3387-3389.
33. Y. Hoshimoto, Y. Hayashi, H. Suzuki, M. Ohashi and S. Ogoshi, *Organometallics*, 2014, **33**, 1276-1282.
34. E. Carmona, J. M. Marin, M. Paneque and M. L. Poveda, *Organometallics*, 1987, **6**, 1757-1765.
35. M. Brookhart, M. L. H. Green and G. Parkin, *Proc. Natl. Acad. Sci.*, 2007, **104**, 6908-6914.
36. W. H. Harman and J. C. Peters, *J. Am. Chem. Soc.*, 2012, **134**, 5080-5082.
37. C. Tsay and J. C. Peters, *Chem. Sci.*, 2012, **3**, 1313-1318.
38. T. He, N. P. Tsvetkov, J. G. Andino, X. Gao, B. C. Fullmer and K. G. Caulton, *J. Am. Chem. Soc.*, 2009, **132**, 910-911.
39. H. Wang, C. Y. Ralston, D. S. Patil, R. M. Jones, W. Gu, M. Verhagen, M. Adams, P. Ge, C. Riordan, C. A. Marganian, P. Mascharak, J. Kovacs, C. G. Miller, T. J. Collins, S. Brooker, P. D. Croucher, K. Wang, E. I. Stiefel and S. P. Cramer, *J. Am. Chem. Soc.*, 2000, **122**, 10544-10552.
40. J. A. Celaje, M. K. Pennington-Boggio, R. W. Flaig, M. G. Richmond and T. J. Williams, *Organometallics*, 2014, **33**, 2019-2026.
41. E. Kogut, A. Zeller, T. H. Warren and T. Strassner, *J. Am. Chem. Soc.*, 2004, **126**, 11984-11994.
42. J. M. Keith and M. B. Hall, *Inorg. Chem.*, 2010, **49**, 6378-6380.
43. D. Devarajan and D. H. Ess, *Inorg. Chem.*, 2012, **51**, 6367-6375.
44. G. J. Kubas, *Chem. Rev.*, 2007, **107**, 4152-4205.
45. J. W. Tye, M. Y. Darensbourg and M. B. Hall, in *Activation of Small Molecules*, Wiley-VCH Verlag GmbH & Co. KGaA, 2006, pp. 121-158.
46. N. Došlić, V. Gomzi, M. Mališ, I. Matanović and J. Eckert, *Inorg. Chem.*, 2011, **50**, 10740-10747.
47. D. Balcells, E. Clot and O. Eisenstein, *Chem. Rev.*, 2010, **110**, 749-823.
48. R. N. Perutz and S. Sabo-Etienne, *Angew. Chem., Int. Ed.*, 2007, **46**, 2578-2592.
49. Y. R. Luo, *Comprehensive Handbook of Chemical Bond Energies*, CRC Press, Boca Raton, FL, 2007.
50. K. C. Lam, T. B. Marder and Z. Lin, *Organometallics*, 2006, **26**, 758-760.
51. M. Puri, S. Gatard, D. A. Smith and O. V. Ozerov, *Organometallics*, 2011, **30**, 2472-2482.
52. W. Scherer, V. Herz, A. Brück, C. Hauf, F. Reiner, S. Altmannshofer, D. Leusser and D. Stalke, *Angew. Chem., Int. Ed.*, 2011, **50**, 2845-2849.
53. F. M. Conroy-Lewis, L. Mole, A. D. Redhouse, S. A. Litster and J. L. Spencer, *J. Chem. Soc., Chem. Commun.*, 1991, 1601-1603.